An Approximate Criterion for Morphological Transformations in Small Vapor Grown Ice Crystals

Jerry Y. Harrington and Gwenore F. Pokrifka

Department of Meteorology and Atmospheric Science, The Pennsylvania State University, University Park, Pennsylvania

Corresponding author: Jerry Y. Harrington, jyh10@psu.edu

ABSTRACT: Observations and measurements show that crystals remain relatively compact at low ice supersaturations, but become increasingly hollowed and complex as the ice supersaturation rises. Prior measurements at temperatures > -25°C indicate that the transition from compact, solid ice to morphologically complex crystals occurs when the excess vapor density exceeds a threshold value of about 0.05 g m^{-3}. A comparable threshold is not available at low temperatures. A temperature-dependent criterion for the excess vapor density threshold ($\Delta\rho_{thr}$) that defines morphological transformations to complex ice is derived from laboratory measurements of vapor grown ice at temperatures below -40°C. This criterion depends on the difference between the equilibrium vapor density of liquid ($\rho_{e\ell}$) and ice (ρ_{ei}) multiplied by a measurement-determined constant, $\Delta\rho_{thr} \simeq 0.27(\rho_{e\ell} - \rho_{ei})$. The new criterion is consistent with prior laboratory measurements, theoretical estimates, and it reproduces the classical result of about 0.05 g m^{-3} above -25°C. Since $\Delta\rho_{thr}$ defines the excess vapor density above which crystals transition to a morphologically complex (lower-density) growth mode, we can estimate the critical supersaturation (s_{crit}) for step nucleation during vapor growth. The derived values of s_{crit} are consistent with previous measurements at temperatures above -20°C. No direct measurements of s_{crit} are available for temperatures below -40°C, however our derived values suggest some measurement-based estimates may be too high while estimates from molecular dynamics simulations may be too low.

1. Introduction

The relative complexity of vapor grown ice crystals is known to depend on the ambient ice supersaturation (s_{amb}, hereafter "supersaturation"). The measurements and observations used to create the early habit diagrams (Nakaya 1951; Kobayashi 1961) showed that crystals tend to remain relatively compact, primarily isometric, and solid at low supersaturation. At higher supersaturations a transformation begins to take place: Hexagonal prisms become thinner with more extreme aspect ratios and hollowing begins on the crystal faces. As liquid equilibrium is approached crystal branches, hollows, and other complex features become pronounced. The transformation from a compact crystal to a crystal with increasing complexity has important consequences for the growth rate and evolution of crystals (Takahashi et al. 1991; Fukuta and Takahashi 1999) and for the radiative properties of crystals that compose clouds (Järvinen et al. 2018b). Though all prior measurements indicate that this transformation is dependent on some measure of the supersaturation, the criterion for when morphological transformations begin has been largely qualitative and confined to small ranges of temperature. No criterion that is valid across a broad range of temperatures has been elucidated. The primary goal of this paper is to set forth an excess vapor density criterion that approximately demarcates the transition from compact crystals to those with a complex morphology caused by vapor growth. By "complex morphology" we mean any crystal form that deviates from a nearly isometric crystal with macroscopically flat faces (i.e. "compact" crystals without hollowing).

Observations and laboratory measurements taken over many years have been used to explore the impact of increasing supersaturation on ice crystal growth forms at a given temperature. While much of this work focused on quantifying whether supersaturation or temperature determined the primary habit forms (Nakaya 1954; Marshall and Langleben 1954; Hallett and Mason 1958; Kobayashi 1960), information was also obtained on the morphological transformations that produce secondary habits. The early work of Nakaya (1954) and Kobayashi (1961) showed that the transformation from compact hexagonal prisms to more complex forms depends on the excess vapor density. This quantity is the difference between the ambient water vapor and ice equilibrium vapor densities ($\Delta\rho_v \equiv \rho_v - \rho_{ei}$), and it is directly related to the supersaturation, $s_{amb} \equiv \Delta\rho_v/\rho_{ei}$. Laboratory measurements (Kobayashi 1960; Rottner and Vali 1974) show that compact, solid crystals give way to hollowed and elongated crystals as $\Delta\rho_v$ rises above a threshold value for the

transformation of $\Delta\rho_{thr} \simeq 0.05$ g m^{-3}. While Kobayashi (1961) was relatively specific in defining $\Delta\rho_{thr}$, other works are less specific usually indicating that a transformation takes place once the supersaturation exceeds a threshold value (s_{thr}) of a few percent at relatively high temperatures (above -20°C, Hallett and Mason 1958; Mason 1993) or 10 to 20% at low temperatures (below -30°C, Bailey and Hallett 2004). These latter results broadly match the excess vapor density threshold of Schnaiter et al. (2016), who used an optical complexity factor to delineate between pristine and complex crystals.

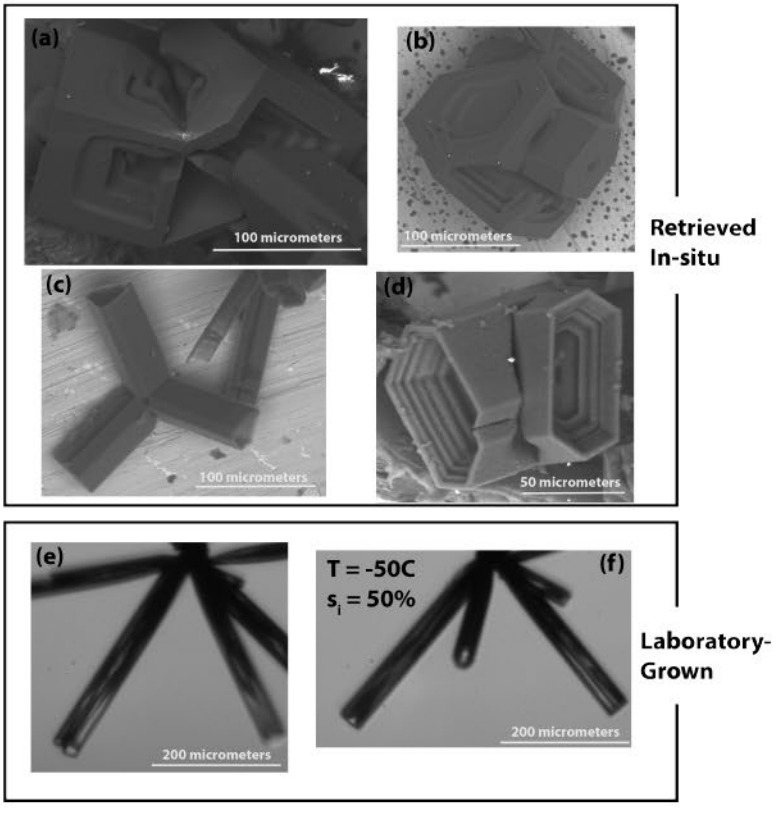

FIG. 1. Small mid-latitude cirrus crystals collected in-situ (at $T \simeq$ -60 to -45°C) with the ICE-Ball sampler and observed with cold stage scanning electron microscopy (a through d, scale bar shown in yellow). (a) and (b) show complex, small, interfused polycrystals with symmetric hollowing and some cubic symmetry (a). Most collected rosettes had hollow arms of either sheaths (c) or scrolls (c, top right). Even the smallest facets were often substantially hollowed (d). Crystals grown in our thermal gradient diffusion chamber from the tip of a fiberglass substrate at -50°C and 50% ambient supersaturation showing (e) a hollow scroll and (f) a hollow column.

Both laboratory measurements and in-situ observations show that crystals, regardless of size, are often hollowed and have complex features. Schmitt and Heymsfield (2007) found that up to 80% of bullet rosettes observed in mid-latitude cirrus showed some degree of hollowing. Even

small ice crystals (diameter < 100 μm) are often complex. While in-situ observations cannot directly visualize the detailed surface structure of small ice, there are indications of complexity in small crystals from imaging and scattering analyses (Järvinen et al. 2018a; Lawson et al. 2019). A recent field campaign (Harrington and Magee 2023) sampled mid-latitude cirrus crystals with the technique of Magee et al. (2021). These studies use balloon-borne capture combined with cold-stage scanning electron microscopy to examine the details of cirrus crystal structure. The observations revealed that many of the sampled crystals are substantially hollowed even at small sizes (Fig. 1a,b,c and d). The majority of rosettes sampled were relatively small, and had hollowed arms composed of either sheaths or scrolls (Fig. 1c). Hollowing must have started when these crystals were much smaller, given the progression of hollowing shown in the images. Morphological transformations appear to be the rule rather than the exception, even for small crystals.

Laboratory measurements show substantial hollowing on larger single crystals and polycrystals at cirrus temperatures (Bailey and Hallett 2004; Smith et al. 2015). We grew crystals from the tip of a 40 μm wide fiberglass substrate in our diffusion chamber (see §3) at a temperature of -50°C and a supersaturation of 50%. The tip of the substrate is dipped in high purity water and inserted into the chamber. Columnar, scroll, and rosette crystals are frequently observed, typically with deep hollowing (see Fig. 1e and f). Experiments with freshly nucleated, small crystals also show indications of morphological transformations above a supersaturation threshold. While newly nucleated crystals can form as classic single crystals, polycrystalline forms are increasingly common at temperatures below -20°C and when crystals are formed from larger supercooled drops (Parungo and Weickmann 1973; Wood et al. 2002; Bacon et al. 2003). Polycrystalline ice tends to remain relatively compact below some threshold in the excess vapor density (Bacon et al. 2003; Pokrifka et al. 2023). Above this threshold, polycrystals have greater complexity (Bacon et al. 2003) and the highest overall growth rates (Pokrifka et al. 2023). Most of the experiments cited above and some theories (Wood et al. 2001) indicate that morphological transformations occur over a relatively broad excess vapor density range near $\Delta\rho_{thr}$, whereas other experiments (Gonda and Yamazaki 1982) and theories (Yokoyama 1993) indicate that a very sharp threshold exists.

Regardless of whether the morphological transformation threshold constitutes a broader range or is a sharp boundary, the value of $\Delta\rho_{thr}$ has important implications for cloud microphysics. Some experimental works have used the 0.05 g m^{-3} threshold to interpret the degree of morphological

complexity that occurs during growth (Bacon et al. 2003), and theoretical models have used it as a benchmark for predictions of when hollowing begins (Wood et al. 2001). The vapor growth theories used in cloud models also make use of this threshold. Numerical cloud models cannot simulate the complex habits of real ice crystals, and so shape approximations are used universally. Generally, ice crystals are treated with an enclosing shape that is either a sphere, an ellipsoid, or a hexagonal prism. The ice mass is then treated with a reduced, or "effective" density (ρ_{eff}) that accounts for regions that do not contain ice. For example, Miller and Young (1979) used the laboratory data of Fukuta (1969) and the 0.05 g m^{-3} threshold to define when ρ_{eff} will decrease during vapor growth. Chen and Lamb (1994) followed a similar approach, but used an exponential form for the density added during depositional growth with crystals remaining solid until the excess vapor density rises above 0.05 g m^{-3}. In all of these approaches, modeled crystals will remain solid at low temperatures, where $\Delta\rho_v = 0.05$ g m^{-3} exceeds liquid equilibrium, which contradicts observational and experimental results.

In this article, we propose an approximate $\Delta\rho_{thr}$ criterion for the initiation of morphological transformations of small, vapor grown ice crystals. The criterion is based on laboratory measurements taken at temperatures below -40°C. We focus our attention on small ice crystals, those with diameters less than about 100 μm, since morphological transformations can begin soon after nucleation, and because the ventilation effects that can enhance branching (Mason 1953) are absent. In the next section (§2), we discuss morphological transformations using facet instability as a working model. In §3 we describe our measurements, define the criterion for morphological transformations ($\Delta\rho_{thr}$), and show that this criterion is consistent with prior measurements and theoretical calculations at higher temperatures (above -30°C). Finally, in §4 we use $\Delta\rho_{thr}$ to provide approximate bounds on the critical supersaturations for faceted growth at temperatures below -40°C.

2. Ice Crystal Vapor Growth and Faceting Instability

Faceting instability[1] has been used to explain the morphological transformation of faceted crystals into hollowed and branched forms (Yamashita 1976; Frank 1982; Nelson 2005). These transformations depend on crystal size, temperature, and pressure (Gonda and Koike 1982; Yokoyama 1993;

[1]While the phrase,"faceting instability", has been used by some authors to refer to this process, it has also been referred to in other ways such as "lacunary catastrophe", "faceting breakdown", "step bunching", "step clumping", and "hollowing".

Mason 1993) but they depend most strongly on the supersaturation (Frank 1982): At relatively low supersaturations facets grow stably meaning that they remain macroscopically flat. As the supersaturation rises, theory and measurements show that the growth conditions for faceting break down leading to the development of hollows and branches (Frank 1982). The results we present in §3 and 4 require a review of faceted growth and faceting instability, and we provide a sketch of those processes here. Our intentions are not to provide a detailed discussion (see Nelson and Baker 1996; Wood et al. 2001; Libbrecht 2017), but rather to provide sufficient information to interpret the latter results.

a. Faceted Growth and Theoretical Model

Faceted growth requires a treatment of both gas-phase vapor and thermal transport processes, and the surface kinetic processes that control the incorporation of adsorbed vapor molecules into the ice lattice. Treating this problem is challenging because the crystal shape, surface kinetics, and gas-phase diffusion are intimately coupled. The growth on a given crystal facet is determined by the flux of water vapor normal to the facet,

$$F_v = \alpha(s_{surf}, T_i)\frac{1}{4}\overline{v}_v[\rho_{surf} - \rho_{ei}(T_i)] = \alpha(s_{surf}, T_i)\frac{1}{4}\overline{v}_v s_{surf}\rho_{ei}(T_i), \tag{1}$$

where $\alpha(s_{surf}, T_i)$ is the deposition coefficient, T_i is the ice crystal temperature, $\overline{v}_v$ is the mean speed of a vapor molecule, ρ_{surf} is the vapor density immediately above the surface, and ρ_{ei} is the ice equilibrium vapor density. Note that the surface excess vapor density, $\rho_{surf} - \rho_{ei}(T_i)$, can be written in terms of the surface supersaturation s_{surf} (rightmost equation). Most of the parameters required to model the crystal surface are not well known, and so the deposition coefficient accounts for all of these processes in aggregate. In the theory of faceted growth (Burton et al. 1951), the surface is thought of as being composed of elementary steps. In this model, adsorbed gas-phase vapor molecules migrate on terraces between steps and ultimately contribute to growth by incorporating into a kink in a surface step. This picture has been modified by theories of quasi-liquid layers that occur on crystal surfaces (Neshyba et al. 2016), but even when these layers exist the "terrace-step-kink" model appears to apply (Murata et al. 2019).

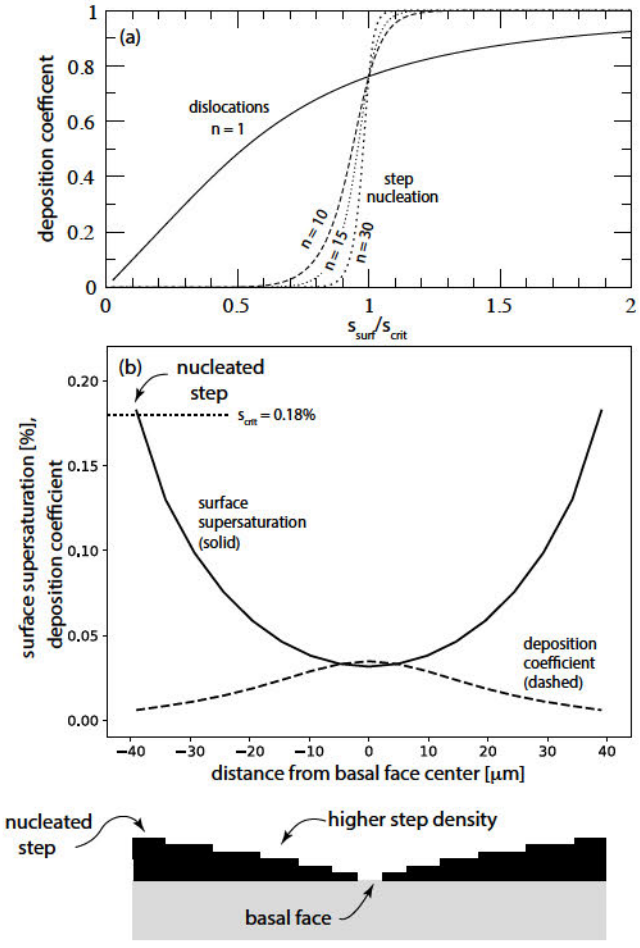

FIG. 2. (a) Deposition coefficient as a function of the surface supersaturation relative to the critical value (s_{surf}/s_{crit}) for dislocation growth ($n = 1$) and growth by step nucleation ($n > 10$). (b) Variation of the surface supersaturation and deposition coefficient from corner-to-corner across the surface of a uniformly growing, 80 μm diameter, basal face. The temperature is -7°C, the supersaturation is 0.3%, and the critical supersaturations for the basal and prism faces are 0.18 and 0.39%, respectively. Steps are nucleated with $n = 10$ shown in (a) near the crystal corners where the s_{surf} is largest (lower cartoon). Steps density is higher as the facet middle is approached, leading to higher α and lower s_{surf}.

Faceted growth requires a model of the deposition coefficient at the step sources. We use the parameterization of Nelson and Baker (1996) that can account for many surface growth modes,

$$\alpha(s_{surf}, T) = \left(\frac{s_{surf}}{s_{crit}(T)}\right)^n tanh\left[\left(\frac{s_{crit}(T)}{s_{surf}}\right)^n\right], \quad (2)$$

where s_{crit} is the critical supersaturation[2] that depends on temperature, and n determines the surface growth mode. Measurements taken over many years (Frank 1982; Nelson and Knight 1998; Libbrecht 2003; Asakawa et al. 2014) indicate that facets generally grow by the two-dimensional nucleation of steps (step nucleation) or dislocations in the crystalline lattice that outcrop on the surface (dislocations) providing a continuous step source. A value of $n = 1$ means that steps are formed by dislocations whereas $n \geq 10$ is used for step nucleation (a value of $n = 10$ is assumed here). Step nucleation requires that the surface supersaturation reach s_{crit} before growth becomes measurable (see Fig. 2a). The deposition coefficient, and growth rate, therefore rises quickly once s_{surf} reaches s_{crit}. In contrast, dislocations provide permanent spiral steps in the crystal surface leading to a gradual increase in α commensurate with the surface supersaturation. In both cases the rise in α is due to increases in the density of steps on the surface.

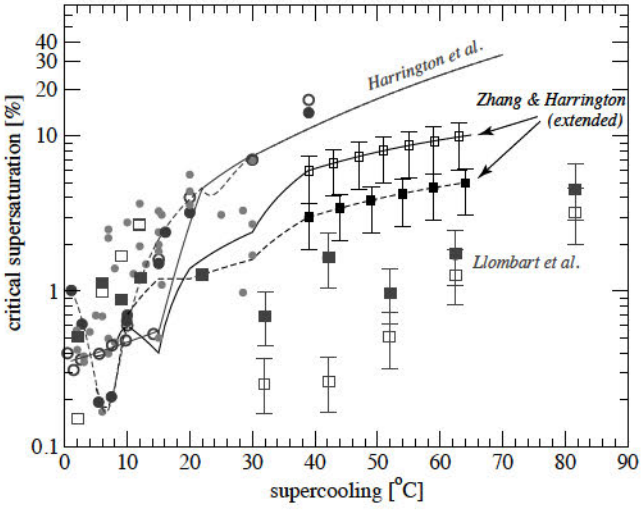

FIG. 3. Critical supersaturation as a function of supercooling ($T_o - T$, where $T_o = 0°C$) for the prism (open circle or square, solid lines) and basal (solid circle or square, dashed lines) faces of ice. The purple circles at temperatures above -15°C are taken from Nelson and Knight (1998) whereas temperatures below -15°C are taken from Libbrecht (2003). Fits to these data points (purple lines) comprise the parameterization of Harrington et al. (2019). Zhang and Harrington (2014) estimates based on fits to growth data are shown as the thin black lines, and extensions to lower temperatures based on the threshold excess vapor density is shown with the black squares. The blue squares are estimated from edge free energies predicted by molecular dynamics simulations (Llombart et al. 2020). The grey circles include all of the remaining data from Harrington et al. (2019).

[2]Note that "critical supersaturation" is typically used for step nucleation only, that "transition supersaturation" is sometimes used for dislocation growth, and "characteristic" supersaturation is sometimes used to refer to both growth modes. We use critical supersaturation because much of our latter discussions focuses on step nucleation.

Using Eq. 2 in models of ice growth requires measurements of s_{crit} as a function of temperature, however these data are sparse, especially at low temperatures. Zhang and Harrington (2014) combined the datasets of Nelson and Knight (1998) and Libbrecht (2003) to produce s_{crit} consistent with Eq. 2 for temperatures down to -40°C (Fig. 3, thin black lines). The measurements of Nelson and Knight (1998) have been remarkably successful in predicting the growth of ice crystals at temperatures above -15°C (Wood et al. 2001; Nelson 2001; Bacon et al. 2003; Zhang and Harrington 2014; Harrington et al. 2019; Harrington and Pokrifka 2021), and is the primary reason Zhang and Harrington (2014) based their fit to s_{crit} on those data.

No direct measurements of s_{crit} are available at temperatures below -40°C, and so Harrington et al. (2019) derived rough approximations based on the laboratory measurements of Magee et al. (2006) and Bailey and Hallett (2004). These s_{crit}values are almost twice as high as Zhang and Harrington (2014) at -40°C. It is also possible to estimate s_{crit} at low temperatures from the step edge free energy (β) predicted by molecular dynamics simulations (Llombart et al. 2020). These predicted values of β are used to calculate s_{crit} with Eq. 3 from Libbrecht (2003), though an effective surface area for the occupying molecule is needed in the relationship. Because the occupying area is not well known, we use average of the theoretical areas for the basal and prism ice lattice spacing (Eqs. 4.13 and 4.14 of Kuroda and Lacmann 1982) with uncertainty bars ranging from the smallest to largest area (blue points, Fig. 3). The estimated values of s_{crit} are similar to some prior measurements above -20°C, but decrease and remain very low below -30°C. This result occurs because the model predicted values of β are substantially smaller than measurements at low temperatures (see Fig. 6 of Llombart et al. 2020). The large range of s_{crit} estimates at temperatures below -30°C is problematic since ice crystal growth and faceting instability depend sensitively on s_{crit} (see §2b). Clearly, measurements of s_{crit} at temperatures below -30°C are sorely needed.

Coupling gas-phase vapor and thermal diffusion with surface processes is a challenging problem. Simplified treatments are available for spherical (Colbeck 1983; MacKenzie and Haynes 1992) and spheriodal (Zhang and Harrington 2014) particles, but these approaches assume a single s_{surf} for either the entire crystal or for each facet. In contrast, measurements (Berg 1938; Humphreys-Owen 1949) and theoretical calculations (Nelson and Baker 1996) show that s_{surf} varies over the crystal faces, and this variation is important for faceting instabilities (see §2b). Theoretical models that

treat s_{surf} appropriately exist for simple shapes such as cylinders (Nelson and Baker 1996) and hexagonal prisms (Wood et al. 2001).

We use the hexagonal prism model of Wood et al. (2001) to couple the gas phase diffusion and surface kinetic problems because the model was successfully used to explain some features of the habit diagram (Wood et al. 2001) and the faceting instability that led to side planes in the measurements of Bacon et al. (2003). The model solves the coupled problem using a triangular grid that spans the basal and prism faces of a single crystal. We use the high resolution treatment of the crystal faces (770 total vertices) even though Wood et al. (2001) showed similar results were obtained for both their low and high resolution grids. The model predicts the location that step nucleation (Eq. 2 with $n = 10$) occurs based on where the surface supersaturation is highest, which is generally the crystal corners (see §2b). Predicting the location of dislocations on crystal surfaces is generally not possible, and so the model presumes a single spiral dislocation source at the facet centers, which is similar to other theoretical treatments (Nelson 1994). While these approximations are rooted in measurements of growing crystals, they are simplifications that should be borne in mind. We discuss how these limitations may bear on our results in the conclusions. For a detailed description of the hexagonal prism model, please see Wood et al. (2001).

b. Faceting Instability

For crystals to grow with a macroscopically flat facet, the vapor flux across each crystal face (Eq. 1) must be constant,

$$\alpha(s_{surf}, T_i)\frac{1}{4}\bar{v}_v s_{surf}\rho_{ei}(T_i) = constant \qquad \text{or} \qquad \alpha(s_{surf}, T_i)\cdot s_{surf} = constant. \tag{3}$$

To maintain a constant vapor flux requires that the surface supersaturation and deposition coefficient vary across the facet. In the theory of faceted growth (Burton et al. 1951), the constancy of $\alpha(s_{surf}, T)\cdot s_{surf}$ is determined by the formation and density of steps on the crystal surface. If the surface step density is high, vapor attachment tends to be efficient, the deposition coefficient is high, and the surface supersaturation is low (Fig. 2b). Conversely, in regions where the step density is low, the deposition coefficient is small, and the surface supersaturation is high (Nelson and Baker 1996). For a nearly isometric crystal, such as those treated below, the surface supersaturation is

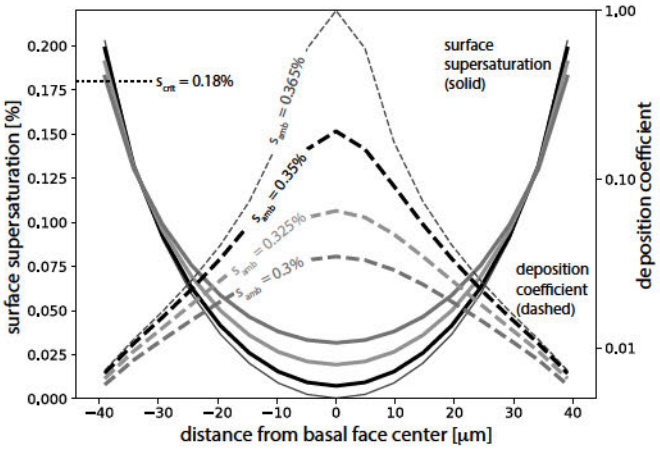

FIG. 4. Variation of the surface supersaturation (solid lines, left y-axis) and deposition coefficient (dashed lines, right y-axis) from corner-to-corner across the surface of the basal face. The ambient supersaturation (s_{amb}) is indicated by color and is labeled on each α curve.The crystal is isometric with $a = c = 40$ μm, the temperature is -7°C, and the critical supersaturations for the basal and prism faces are 0.18 and 0.39%, respectively.

highest near the crystal corners, it is lower near the crystal edges, and smallest over the facet centers (Nelson and Baker 1996; Libbrecht 2005).

Stable faceted growth can be maintained as long as the deposition coefficient remains below unity, which occurs at relatively low surface supersaturation. Consider a crystal growing by step nucleation (via Eq. 2 with $n = 10$) computed with the model of Wood et al. (2001) for a pressure of 1000 hPa, a temperature of -7°C, and a supersaturation of 0.3%. The crystal is small with 40 μm semi-dimensions (half the distance across the basal face and half the height of the prism face). The variation in s_{surf} and α from corner-to-corner across the basal face is shown in Fig. 2b. Step nucleation occurs preferentially near the corners because the surface supersaturation maximizes there and minimizes at the facet center. Because $\alpha(s_{surf}, T) \cdot s_{surf}$ must remain constant, the deposition coefficient has a minimum at the corners and a maximum at the facet center. This result is consistent with the theory of step nucleation and propagation that underlies Eqs. 2 and 3: Steps nucleate near the corners and propagate parallel to the face. Since the surface supersaturation is lower over the facet center, the steps slow down as they approach the center, the density of steps increases and the deposition coefficient therefore rises thus keeping $\alpha(s_{surf}, T) \cdot s_{surf}$ constant (see cartoon in Fig. 2b).

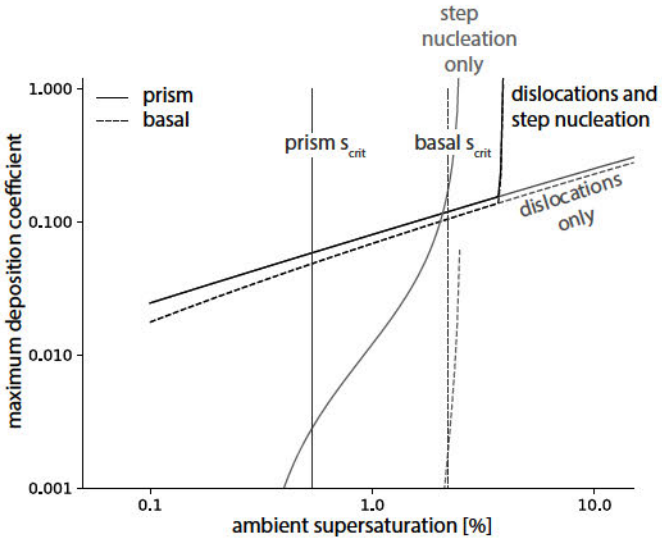

FIG. 5. Maximum value of the deposition coefficient on the prism (solid) and basal (dashed) faces as a function of the ambient supersaturation for an isometric crystal with a semi-dimension of 40 μm, and at a temperature and pressure of -15°C and 1000 hPa respectively. Growth by dislocations only (green lines), dislocations and step nucleation (black lines), and step nucleation only (red lines) are shown. Faceting instability occurs when step nucleation is possible (α approaches unity) and when the ambient supersaturation is above the highest critical supersaturation (vertical blue lines).

Faceting instability occurs when it is no longer possible for $\alpha(s_{surf}, T) \cdot s_{surf}$ to remain constant. As the supersaturation rises, step nucleation near the corners increases leading to a higher density of steps propagating toward the facet center (Fig. 4). At some value of the surface supersaturation near the corner, step nucleation and growth becomes rapid enough that steps bunching near the facet centers drive the surface supersaturation to zero and α to unity (purple line in Fig. 4). When this condition occurs, the criterion for stable faceted growth breaks down. Steps can no longer propagate inward leading to the development of a "step clumping region" (Nelson 2005) and a hollow develops at the facet center. Bacon et al. (2003) refer to this as a "faceting instability" whereas Frank (1982) calls it a "lacunary catastrophe" that becomes more pronounced as the supersaturation rises further. Indeed, Frank (1982) shows how this lacunary catastrophe can be used to explain hollowing and the development of branches on stellar crystals. Three-dimensional models capable of growing crystals once hollowing occurs produce surface supersaturation distributions and faceting instabilities that are consistent with this picture (Barrett et al. 2012). For the example shown in Fig. 4, this instability occurs when $s_{amb} \simeq 0.365\%$, which is the threshold supersaturation (s_{thr}) discussed above. This value of s_{amb} is just below s_{crit} for the prism face (0.387%) and is about 2 times the s_{crit} of the

basal face (0.18%) at -7°C. This result is similar to the criterion that Wood et al. (2001) found for hollowing when crystals grow by step nucleation. Faceting instability can occur also occur by dislocation step sources at the crystal edges, although at a lower threshold supersaturation (Bacon et al. 2003, see their Fig. 12).

Even though the example above uses step nucleation, faceting instability also occurs if crystals grow initially by dislocations originating at the facet centers, such as during spiral dislocation growth (Wood et al. 2001). Most crystals formed in atmospheric cold clouds likely have numerous defects in the crystal lattice produced during nucleation. Real crystals, therefore, probably grow initially by dislocations (Nelson 2001; Bacon et al. 2003; Lamb et al. 2023) but transition to step nucleation growth at high supersaturation (Frank 1982; Nelson and Knight 1998). For example, Fig. 5 shows the maximum value of the deposition coefficient on each facet as a function of s_{amb} for a growing isometric crystal at a temperature and pressure of -15°C and 1000 hPa, respectively. Recall that the maximum value of the deposition coefficient is not necessarily near the corner, but can be at the facet center (Fig. 4). The surface supersaturation rises commensurately with s_{amb} and when s_{crit} is reached, step nucleation occurs and α rises rapidly (black lines, Fig. 5). Once step nucleation occurs, the propagation of steps towards the facet center leads to the same lacunary catastrophe described above for step nucleation growth only, albeit at a higher s_{amb} (compare red and black lines, Fig. 5). Higher supersaturations are required to initiate faceting instability when dislocations are present because the high density of steps keeps s_{surf} lower over the corners. It is worth noting that crystal growth is generally stable if crystals grow exclusively by dislocations originating at the facet centers. In this case, α rises continually with s_{amb} up to liquid equilibrium yet α never reaches unity (green lines). Such growth is therefore stable at all supersaturations, and faceting instability does not occur. Consequently, *step generation near the crystal corners and edges is required for the initiation of faceting instability.*

Following Wood et al. (2001) and Bacon et al. (2003), we use faceting instability to describe the initial onset of morphological transformations in small, vapor grown ice crystals. Though we use the theory described above, it is worth keeping in mind that the theoretical model is strictly valid for single crystals. We nevertheless use the model to interpret growth data from both single crystals and ice formed from frozen droplets in §4. The resulting crystals from these latter experiments are likely polycrystalline with facets that intersect at non-crystallographic angles (see Fig. 1). Hence,

the supersaturation distribution over the crystal faces will be different than that predicted by the single crystal model. The interpretations derived from the model should therefore be viewed as approximate and qualitative. Nevertheless, as we will show, the results still have explanatory power.

3. Morphological Growth Transitions in Laboratory Measurements

The measurements and theoretical calculations described in the last two sections indicate that crystals undergo a morphological transformation from compact to increasingly complex as the excess vapor density rises above a threshold value of about 0.05 g m^{-3} at temperatures above -25°C. However, measurements indicate that $\Delta\rho_{thr}$ is far lower at temperatures below -40°C (Bailey and Hallett 2004; Schnaiter et al. 2016). We are therefore left with a question: *Can a general form for $\Delta\rho_{thr}$ be found that is approximately valid at low and high temperatures?* In this section, we show results from laboratory growth experiments and use those experiments to come up with an approximate, but general criterion for morphological transformation based on crystal effective density.

a. Prior Experimental Data

Measurements in ice crystal growth chambers provide quantitative data on, and an explicit criterion for, morphological transformation. At temperatures above -10°C, Colbeck (1983) grew crystals in a thermal gradient diffusion chamber and showed that at low supersaturation crystals had rounded forms consistent with the equilibrium shapes of crystals at temperatures near the melting point. As the supersaturation was increased, compact faceted forms appeared first which were followed by hollowed crystals (their data are shown in Fig. 6). Bacon et al. (2003) used measurements of ice crystals grown in a levitation diffusion chamber to estimate the supersaturation at which morphological transformations take place. Their experiments showed that crystals became "florid" (meaning that side planes developed through faceting instability) once the excess vapor density increased above about 0.05 to 0.1 g m^{-3} (Fig. 6). Their data show that compact crystals do still exist above this threshold, however hollowing undetected by the imaging methods may have occurred on some of the crystals.

Using a subset of their growth data for more pristine, presumably single crystals, Bacon et al. (2003) estimated the excess vapor density at which faceting instability occurred ($\Delta\rho_{thr}$), and this

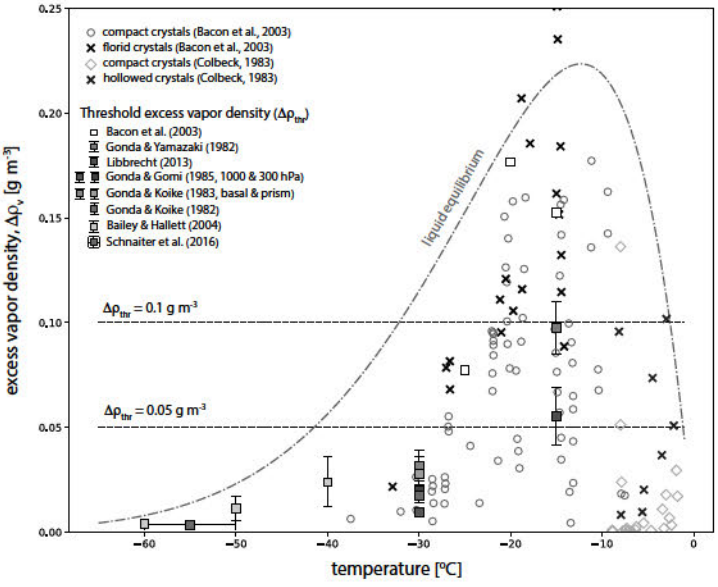

FIG. 6. Measurements of compact crystals (open circles and diamonds), and florid/hollow crystals (crosses, black and blue) as a function of temperature and excess vapor density. Estimates of the excess vapor threshold ($\Delta\rho_{thr}$) estimated from prior measurements are shown by the colored squares (see legend and Table 1. Also shown (black dashed lines) is the often-used threshold of $\Delta\rho_{thr}$ = 0.05 g m^{-3}, and the 0.1 g m^{-3} threshold discussed in Bacon et al. (2003). The excess vapor density at liquid equilibrium, which is approximately the maximum value in atmospheric clouds, is also shown (red dot-dashed line).

coincided roughly with the appearance of florid crystals in their experiments (squares, Fig. 6). Their theoretical results indicated that no strong size dependence of $\Delta\rho_{thr}$ exists, and that the transition from compact to florid crystals occurs over a broad range near $\Delta\rho_{thr}$ due to the range of growth mechanisms and differences in small-scale morphology that likely occurred in their experiments (see Fig. 12 of Bacon et al. 2003).

In contrast to the results of Colbeck (1983) and Bacon et al. (2003), the cloud chamber experiments conducted by Gonda and co-workers showed a relatively sharp, size- and pressure-dependent threshold for faceting instability. While some studies provide the criterion for morphological transformation in terms of the excess vapor density ($\Delta\rho_{thr}$), other studies use a supersaturation threshold (s_{thr}). The cloud chamber experiments of Gonda and Yamazaki (1982) showed a relatively sharp s_{thr} for the transition from compact polyhedral growth to skeletal (hollowed) and finally to dendritic growth at -15°C (see their Fig. 3). The numbers extracted from their experiments, and others, are given in Table 1 and are shown on Fig. 6 as excess vapor density thresholds. To estimate s_{thr} we extracted the lowest value from actual data-points in the figures (not interpolated or extrapolated

TABLE 1. Threshold supersaturation (s_{thr}) for faceting instability from prior studies. Pressure and habit type are noted when known.

temperature (°C)	s_{thr} (% or ppmv)	uncertainty, Δs_{thr} (% or ppmv)	pressure/habit	source
-15.0	7.03%	0.89%	1000 hPa, planar	Gonda and Yamazaki (1982)
-15.0	4.0%	1.0%	planar, estimate	Libbrecht (2013)
-30.0	5.1%	1.0%	1000 hPa, planar	Gonda and Koike (1982)
-30.0	9.40%	2.14%	columnar, basal face	Gonda and Koike (1983)
-30.0	8.21%	2.38%	planar, prism face	Gonda and Koike (1983)
-30.0	2.84%	0.64%	1000 hPa, columnar	Gonda and Gomi (1985)
-30.0	5.83%	0.84%	300 hPa, columnar	Gonda and Gomi (1985)
-40.0	15.0%	10.0%	300 hPa, multiple forms	Bailey and Hallett (2004)
-50.0	30.0%	15.0%	250 hPa, multiple forms	Bailey and Hallett (2004)
-60.0	35.0%	15.0%	200 hPa, multiple forms	Bailey and Hallett (2004)
-55.0	4.318 ppmv	2.0 ppmv	1000 to 800 hPa	Schnaiter et al. (2016)

lines). This procedure provides s_{thr} for the first indication of a morphological transformation. Since Gonda and co-worker's data shows a moderate size dependence, with an extrapolated minimum below their lowest s_{thr} measurement, we estimated the uncertainty ranges by taking the distance from the data point to this minimum. The minimum occurs in the semi-dimension range of about 30 to 80 μm for all of their experiments (Gonda and Koike 1982, 1983; Gonda et al. 1984; Gonda and Gomi 1985), which is in the size range when most atmospheric crystals may experience faceting instability early in their growth. The error bars therefore provide information on the size-dependence of these data. We used this approach for all of Gonda and co-worker's data. Libbrecht (2013) showed experimentally that a plate-on-plate growth instability occurred at -15°C once the supersaturation rose above about 4 to 5%. The thresholds derived from these experiments and numerical studies at -15°C generally match the $\Delta\rho_{thr}$ of 0.05 to 0.1 g m^{-3} criterion for morphological transformations (Fig. 6).

At lower temperatures $\Delta\rho_{thr}$ declines, as is apparent from the growth data of Gonda and co-workers (Figs. 7, 5, 3 from Gonda and Koike 1982, 1983; Gonda and Gomi 1985, respectively). These cloud chamber studies were done at -30°C, and like their experiments at -15°C the data also show a generally sharp, size- and pressure-dependent transition from a compact, polyhedral crystal to a hollowed crystal above s_{thr}. The experiments showed that s_{thr} is generally in the range of 3 to 10% (see Table 1 and Fig. 6).

Experiments at cirrus temperatures (below about -40°C) are rare, though Bailey and Hallett (2004) provided a rich data set from their diffusion chamber experiments. At temperatures near -40°C, substantial rosette growth seemed to occur above a supersaturation of about 15% and we use this as an approximate threshold at this temperature with an uncertainty range of 10%. At -50°C Bailey and Hallett (2004) found that rosettes appear at a supersaturation of about 20% and columns hollow at around 40% supersaturation, whereas at -60°C these two supersaturations are about 25% and 50%, respectively. These numbers provide a broad range of supersaturation over which morphological transformations take place, and the mid-point and range are given in Table 1 and Fig. 6. The transformation from compact to complex polycrystalline ice shown by the experiments of Bailey and Hallett (2004) are consistent with the increases in optical complexity of ice grown in the expansion cloud chamber experiments of Schnaiter et al. (2016). Their work showed that crystals transition from "pristine" to "complex" once an optical complexity factor exceeds a threshold of 4.6. Equation 2 of Schnaiter et al. (2016) indicates that this optical threshold occurs at a vapor mixing ratio of about 4.318 ppmv (see Table 1). This threshold is shown in Fig. 6 with uncertainty bars including the range of temperature (about -50°C to -60°C) and pressure (900 to 700 hPa) of the expansion experiments. Though the results from Bailey and Hallett (2004) are qualitative, they do tend to fall within the range of the quantitative information from Schnaiter et al. (2016) (as these latter authors noted). The thresholds derived from these data also decrease with the temperature. It is curious that the data appear to roughly follow the line for liquid equilibrium (red dot-dashed line, Fig. 6), and this provides a key to a general criterion for $\Delta\rho_{thr}$.

b. Low-Temperature Measurements and a New Criterion for $\Delta\rho_{thr}$

We conducted a relatively large number of individual ice crystal growth experiments (approximately 300) at temperatures ranging from -65 to -40°C and at ambient atmospheric pressure of 970 hPa (Pokrifka et al. 2023) . The apparatus is a thermal gradient diffusion chamber combined with electrodynamic levitation (see Harrison et al. 2016, for a detailed description). The temperature and vapor pressure of the environment are static, and are controlled by different temperatures on the upper (warmer) and lower (colder) copper plates. The plate temperatures are controlled by two Ultra Low Temperature (UTL) thermal baths, with temperature monitored by thermocouples underneath the inner surfaces of the copper plates. Supersaturation is produced by coating both

plates with ice and a three dimensional diffusion model of the chamber is used to compute the supersaturation. Charged liquid water droplets are launched into the chamber through a small opening in the upper copper plate and are levitated with an adjustable voltage applied to the bottom plate. The droplet freezes rapidly at the low chamber temperature. Lateral stability is provided by an alternating current (AC) applied to four small button electrodes attached to the top plate. Electrically enhanced growth is unlikely given that the charge on the particle is relatively low (Harrison et al. 2016). While particles can undergo slow rotation in the electric field and we expect that any influences on growth should be small: As Pokrifka et al. (2023) showed, and as we show below, growth at low supersaturations frequently show kinetic limitations with a functional form of the growth rate that is similar to that of a sphere. If particle rotation strongly influenced growth we would expect to see a deviation from the aforementioned growth, particularly as a particle grows larger. Moreover, the force from the quadrupole electrodes is radially directed and lacks a tangential component, which matches our observation that regions of bright reflection, presumably due to facets, move slowly back and forth often taking minutes to transect the 20 degree field of view. The initial radius (and mass, $m_\circ$) of the particle is determined to within ~ 1 μm from Mie scattering analysis of the diffraction pattern resulting from laser illumination of the levitated crystal. Most of our crystals have an initial radius between 9 and 15 μm. Stable levitation is maintained by software that monitors and continuously adjusts the levitation voltage. Since the only vertical forces acting on the particle are electrostatics and gravity, the mass ratio ($m_r \equiv m/m_\circ$) can be determined directly and relatively precisely (to within 2.5% error) from the measured voltage. Note that we cannot capture images of the levitated particles, and so morphological changes must be inferred from the measured growth rate (Pokrifka et al. 2023).

Our experiments ranged from very low supersaturations to supersaturation near that of liquid equilibrium. We found that the crystals in our experiments had growth rates that were best explained by a model of polycrystalline budding rosettes though up to 30% of the growth data could be explained by columns (Pokrifka et al. 2023). This result is consistent with prior measurements that show a preponderance of polycrystalline ice at low temperatures, though small drops (radii $<$ 10 μm) can still freeze as single crystals (Parungo and Weickmann 1973; Pitter and Pruppacher 1973; Bailey and Hallett 2004). Because our crystals begin as frozen droplets presumably with numerous defects, we compare the measured growth rates to the diffusion-limited rate of a solid

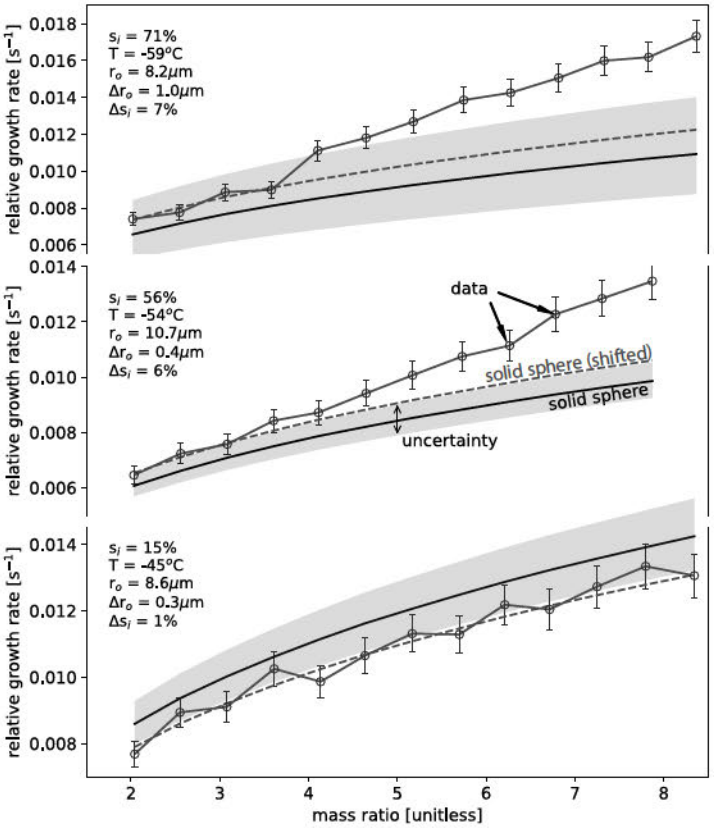

FIG. 7. Relative growth rate, $\frac{d}{dt}\left(\frac{m}{m_o}\right)$, as a function of the mass ratio $\left(\frac{m}{m_o}\right)$ derived from levitation diffusion chamber measurements at three different temperatures and supersaturations (given in the legends). Data points are given by the purple circles and solid green lines. Calculations assuming a solid spherical crystal are shown as the solid black lines with the uncertainty (Δr_o) in the initial radius (r_o) show by the blue shade. The dashed green line shows the spherical model solution shifted such that it matches the early growth of the crystals, making it easier to discern when the measured growth rate deviates from the spherical rate. This deviation generally occurs when $\frac{m}{m_o} > 3.5$ for the growth at higher supersaturation (middle and upper panel), indicating a possible morphological transformation.

sphere (i.e with perfect attachment kinetics or $\alpha = 1$). The growth rates of the measured crystals deviated substantially from that of a solid sphere (or compact crystal) once the supersaturation increased above a certain threshold (Pokrifka et al. 2023). For example, Fig. 7 shows the mass growth rate relative to the initial mass (dm_r/dt) as a function of the mass ratio (m_r) for three typical experiments out of the set of nearly 300. We use m_r as the abscissa instead of time since crystals grown at low supersaturation require a much longer time to reach a large mass ratio. While each experiment was conducted at a different temperature, the figure clearly shows that when the supersaturation is low (lower panel) the measured growth rate is quite close to that of a solid sphere.

At higher supersaturations (middle and upper panels), a change in the growth rate occurs. Note that at $m_r \sim 3$ to 3.5 the growth rate begins to deviate from that of a solid sphere, and increases as the crystal grows larger. Where the deviation begins is made clearer by shifting the growth curve for a solid sphere so that it matches, on average, the early growth rates of the measured crystals (green dashed line). This deviation in the growth rate indicates that a morphological transformation has taken place (Pokrifka et al. 2023): Rosette arms may develop, hollow, and extend into the vapor field, or column crystals may develop and hollow. Each of these processes will drive the growth rate upwards, and in Pokrifka et al. (2023) we parameterized this growth enhancement with an enclosing sphere and an "effective" density (ρ_{eff}) that implicitly accounts for the increase in complexity (arms and hollows) of the crystals. Pokrifka et al. (2023) used both the deposition density method of Chen and Lamb (1994) and a power-law to determine ρ_{eff} by fitting the growth data. In this manuscript, we use ρ_{eff} determined from the deposition density method. Since both methods produce nearly the same average growth rates, our results are not influenced by this choice.

Modeling complex ice with an enclosing sphere and an effective density has limitations (see Pokrifka et al. 2023) that are worth keeping in mind: At low supersaturations frozen droplets will develop facets over time and, perhaps, complex though compact morphology (Gonda and Yamazaki 1984; Takahashi and Mori 2006). Using a sphere to model the growth will naturally convolve surface kinetic effects with morphological change. This limitation should primarily impact the determination of the deposition coefficient (see Harrington and Pokrifka 2021), and therefore should have minimal impact on the determination of whether crystals are compact with a high ρ_{eff}. At high supersaturations, we expect arms and hollowed regions to develop. Since these are all treated with an effective density, any impacts that rosette arm development and hollowing may have on the growth rate will be convolved with ρ_{eff}.

Our experimental data showed that the transformation from compact, higher effective density crystals to low effective density crystals occurred at a supersaturation relative to liquid equilibrium (see Fig. 12 of Pokrifka et al. 2023). We will refer to this quantity as the relative excess vapor density[3], σ,

$$\sigma \equiv \frac{\rho_v - \rho_{ei}}{\rho_{e\ell} - \rho_{ei}} = \frac{\Delta\rho_v}{\Delta\rho_{liq}}. \tag{4}$$

[3]In Pokrifka et al. (2023) we refer to this as the "supersaturation ratio", $s_{i,rat}$.

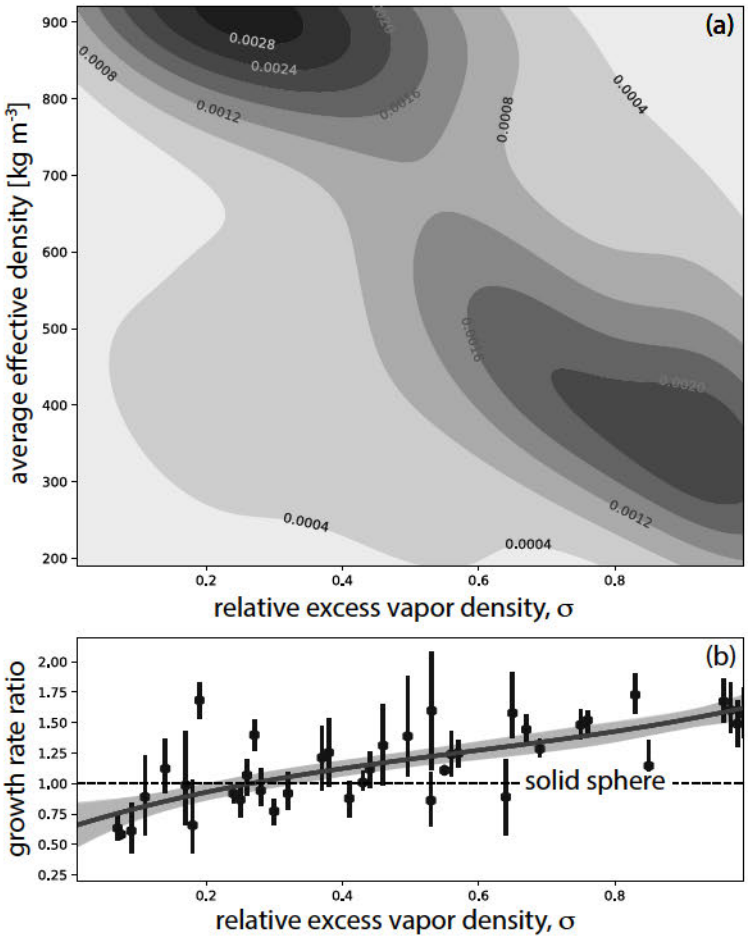

FIG. 8. (a) Two dimensional distribution of diffusion chamber measurements of average effective density (ρ_{eff}) and relative vapor excess ($\sigma \equiv \frac{\rho_v - \rho_{ei}}{\rho_{e\ell} - \rho_{ei}}$) and (b) the measured growth rate divided by the diffusion-limited rate of a solid sphere (growth rate ratio) dependence on relative vapor excess. Values below the black dashed line indicate kinetic limitations to growth, whereas values above this line indicate growth enhancement due to morphological change. The data points are averages of the experimental data divided into 40 bins. The error bars give the 95% confidence interval around the average value. The purple curve is a 3^{rd}-order polynomial fit to the data with the shading indicating the 95% confidence interval in the fit.

The numerator is the excess vapor density discussed above. The denominator ($\Delta\rho_{liq}$) contains the difference between the liquid ($\rho_{e\ell}$) and ice equilibrium vapor densities. This difference is approximately the maximum excess vapor density that can be attained in atmospheric clouds, including in cirrus when homogeneous freezing occurs. When all of our experimental growth data (see Pokrifka et al. 2023, for details) are plotted against σ a broad range of growth rates and ρ_{eff} are found to occur (Fig. 8) with a general transition from compact crystals with low growth rates at low σ to crystals with lower effective densities and higher growth rates at high σ. Pokrifka et al.

(2023) showed that this broad range of growth rates and densities could be explained by crystals with varying morphology. Fits to these growth data by Pokrifka et al. (2023) indicate that the transition from compact crystals to complex crystals occurs in a region around $\sigma \simeq 0.27$ (Fig. 8). Note that for $\sigma < 0.2$ crystals are well modeled with a compact, isometric shape with high ρ_{eff}. This result is also evident in Fig. 7: The measured growth rates have a similar functional form as that of a solid sphere growing at the diffusion-limited rate (green dashed line) but with a lower overall rate (black line), indicating surface kinetic limitations (Fig. 8b). Crystal effective densities decrease and growth rates increase, once $\sigma >$ about 0.4. We selected the upper and lower limits of this range somewhat subjectively, but reasonably: The number of experiments that indicate growth limited by surface kinetics increases as σ declines. About 60% of experiments show indicates of surface kinetic limitations to growth at $\sigma = 0.2$, whereas only about 30% of cases show kinetic limitations at $\sigma = 0.4$. While this is a broad range of relative excess vapor density (0.2 to 0.4), these results are consistent with broad range of $\Delta\rho_{thr}$ found by Bacon et al. (2003).

The results above suggest that a general, temperature-independent threshold for morphological transformations is approximately,

$$\begin{aligned} \sigma_{thr} &\simeq 0.27 \qquad \text{within the range 0.2 to 0.4,} \\ \Delta\rho_{thr} &= \sigma_{thr}\Delta\rho_{liq}. \end{aligned} \tag{5}$$

In other words, the measurements suggest that a criterion for morphological transformation ($\Delta\rho_{thr}$) can be written in terms of a temperature-independent constant multiplied by the excess vapor density at liquid equilibrium. This criterion and range (purple line and shade, respectively) are shown on Fig. 9a along with the measurements from Fig. 6 and our effective density data. The new criterion separates the high density, compact crystals from the lower density, complex crystals at low temperatures, as expected. The new criterion also demarcates the higher temperature results from Bacon et al. (2003) and, to a lesser extent, Colbeck (1983). Moreover, at temperatures between -5 and -25°C, Eq. 5 reproduces, in approximation, the excess vapor density threshold of about 0.05 g m^{-3}. The range of $\Delta\rho_v$ over which morphological transformations are predicted to begin is also quite similar to the range of about 0.05 to 0.1 g m^{-3} implied by Bacon et al. (2003). At lower temperatures, Eq. 5 approaches the threshold supersaturation of about 20%, which Schnaiter

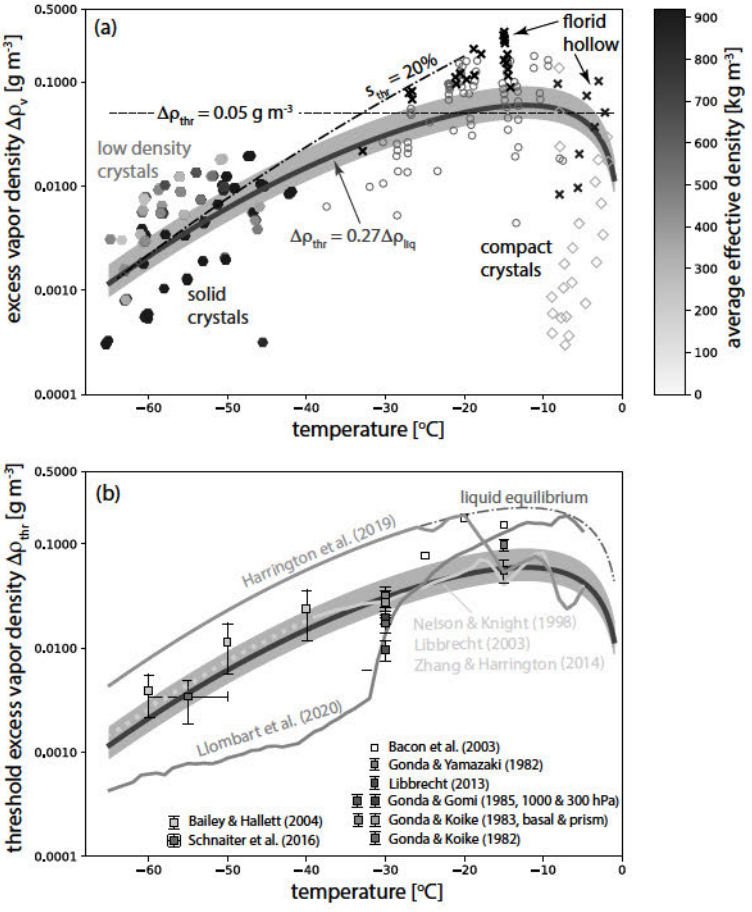

FIG. 9. (a) Measurements from Fig. 6 along with the measurements of Pokrifka et al. (2023) shaded with effective density (note that there are overlapping data points). Also shown (black dashed lines) is the often-used threshold of $\Delta\rho_{thr}$ = 0.05 g m^{-3} and s_{thr} of about 20% that appears consistent with some low temperature measurements. The $\Delta\rho_{thr}$ from Pokrifka et al. (2023) along with the 0.2 to 0.4 range is shown by the purple line and shade, respectively. A log scale is used so that the $\Delta\rho_v$ at lower temperature are clear. (b) Excess vapor threshold ($\Delta\rho_{thr}$) from Fig. 6 along with the threshold and range from Pokrifka et al. (2023). Theoretical calculations of $\Delta\rho_{thr}$ using critical supersaturation data sets from Zhang and Harrington (2014)(green lines), the data of Harrington et al. (2019) (gold line), and the molecular dynamics simulation results of Llombart et al. (2020) (rose line). The transition from the green solid to dotted line shows the s_{crit} from Zhang and Harrington (2014) extended to temperatures below -40°C.

et al. (2016) and Bailey and Hallett (2004) noted separates pristine crystals from the development of complex particles. This new threshold also better matches the values of $\Delta\rho_{thr}$ determined from prior experiments, as shown on Fig. 9b. However, some of the measurements at -30°C are substantially lower than the smallest estimate (σ_{thr} = 0.2) using Eq. 5. The estimate from Schnaiter et al. (2016) falls in the middle of Eq. 5 as do the lower end of the estimates from the data of Bailey and Hallett (2004). The correspondence of these prior studies with our results (Pokrifka

et al. 2023) is encouraging, since they indicate that the transformation from compact to complex crystals occurs over a similar range of $\Delta\rho_v$ for different experiments.

Though all of the data above fall within the broad range of $\Delta\rho_{thr}$ estimated by Eq. 5, it is important to keep in mind that equation 5 is based on diffusion chamber measurements in which budding rosettes and hollowed single crystals likely occurred. So this equation probably describes when substantial branching and hollowing occurred on the crystals (Pokrifka et al. 2023): It tells us when the growth rates rose substantially, which indicates a morphological transformation causing the crystals to deviate from spherical growth. This transformation has clear differences from the hollowing and side-plane transformations that the experiments of Colbeck (1983), Gonda and co-workers, and Bacon et al. (2003) showed. It is therefore curious that results from Eq. 5 broadly match all of these data. This correspondence may be due to a general transition from dislocation to step-nucleation mediated growth near the crystal corners. This transition seems to be a necessary (but probably not sufficient) condition for hollowing to commence, for substantial aspect ratios to develop in column crystals and the arms of rosettes, and for the development of intricate surface patterns (Frank 1982; Nelson 2001). We therefore emphasize that many growth features are convolved in our measurements, and this likely leads to a broad range of σ over which a transformation occurs.

4. Theoretical Calculations of $\Delta\rho_{thr}$ and Critical Supersaturations

Wood et al. (2001) used the critical supersaturations of Nelson and Knight (1998) and predicted that the transition from compact to hollowed crystals was consistent with prior habit diagrams, and occurred above an excess vapor density of about 0.05 g m^{-3}. However, the critical supersaturation data at temperatures between -20 and -40°C were not available when their work was published. It is therefore natural to ask how predictions of $\Delta\rho_{thr}$ using recent s_{crit} data compare to the empirical threshold (σ_{thr}) derived from the measurements above.

The excess vapor density threshold can be determined for single crystals from the model of Wood et al. (2001) by increasing the supersaturation until the deposition coefficient reaches unity on the fastest growing facet. Once this occurs, $\Delta\rho_{thr}$ has been reached, faceted growth breaks down and hollowing should commence. Since faceting instability depends on s_{crit}, we conducted simulations with the s_{crit} data from Zhang and Harrington (2014) and Harrington et al. (2019),

along with the values calculated from Llombart et al. (2020). Simulations followed those shown in Fig. 5 for a crystal that transitions from dislocation to step-nucleation mediated growth: The crystal size, shape, and temperature are kept constant, and the supersaturation is increased until faceting instability occurs (i.e. $\alpha = 1$). Using the s_{crit} data from Zhang and Harrington (2014) in the model simulations predict a $\Delta\rho_{thr}$ (green solid line, Fig. 9b) with surprisingly good agreement to the value determined from measurements (Eq. 5). At temperatures above -20°C, the model calculations also generally match the results of both Wood et al. (2001) and Bacon et al. (2003) in that $\Delta\rho_{thr} \simeq 0.05$ g m^{-3}. This correspondence is not surprising since those authors used the same s_{crit} values at higher temperatures that we use here. The green dashed line shows the extension of Zhang and Harrington (2014) to lower temperature (see below).

The s_{crit} values from Harrington et al. (2019) at temperatures above -20°C are similar to those from Zhang and Harrington (2014), and so it is not surprising that the model simulations produce similar $\Delta\rho_{thr}$ (gold curve, Fig. 9b). However, at temperatures below -20°C model predictions of $\Delta\rho_{thr}$ indicate that in order for morphological transformations to occur, the excess vapor density would have to exceed liquid equilibrium. Since hollowing is frequently found on small atmospheric crystals even at low temperatures (Fig. 1), if the s_{crit} values from Harrington et al. (2019) are correct, then these crystals must have grown in an environment near liquid equilibrium. While this could be true for some crystals, most cirrus have supersaturations that fall well below liquid equilibrium (Krämer et al. 2020). Taken together, these results imply that the s_{crit} values from Harrington et al. (2019) are possibly too high at temperatures below -20°C. On the other hand, using the s_{crit} values calculated with the step free energies of Llombart et al. (2020) produce values of $\Delta\rho_{thr}$ that approach liquid equilibrium at temperatures above -15°C, and values of $\Delta\rho_{thr}$ that are very low at temperatures below -30°C (rose curve, Fig. 9b). If $\Delta\rho_{thr}$ were indeed this low (supersaturations less than 0.1%), it would seem that maintaining facets would not be possible in cirrus clouds. The correspondence between estimates of $\Delta\rho_{thr}$ from measurements and model predictions using the s_{crit} data from Zhang and Harrington (2014) provide some circumstantial evidence supporting those s_{crit} data.

The data of Pokrifka et al. (2023) and Eq. 5 suggests that σ_{thr} is a more general criterion for morphological transformations than $\Delta\rho_{thr}$ since it appears to be temperature independent. The σ_{thr} threshold predicted using the different s_{crit} data-sets are shown in Fig. 10. The s_{crit} data of

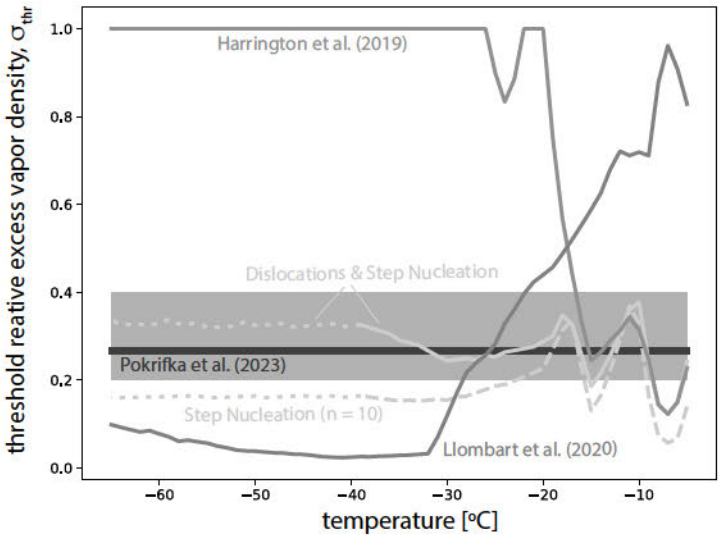

FIG. 10. Threshold relative excess vapor density as a function of temperature from the measurements of Pokrifka et al. (2023) including the 0.2 to 0.4 range (purple line and shade, respectively). Predicted values of σ_{thr} using critical supersaturation data sets from Zhang and Harrington (2014) (green lines), the data of Harrington et al. (2019) (gold line), and the molecular dynamics simulation results of Llombart et al. (2020) (rose line). All predictions use dislocation and step nucleation growth with the model of Nelson and Baker (1996). To demonstrate the possible range of σ_{thr} calculations with step nucleation only are also shown (green dashed). The s_{crit} of Zhang and Harrington (2014) are extended to temperatures below -40°C, and are shown by the continuation of the green solid and dashed lines with the green dotted lines.

Zhang and Harrington (2014) produces a threshold value of σ that ranges between about 0.18 and 0.34 (comparable to Eq. 5) at temperatures below -20°C depending on the growth mechanism used. If crystals grow by step nucleation only, then faceting instability would occur, and crystal complexity would rise, at a relatively low supersaturation (green dashed line, Fig. 10). If crystals grow initially by dislocations and transition to step nucleation as the supersaturation rises, then faceting instability would occur at a higher supersaturation (green solid line, Fig. 10). These model calculations suggest that the broad range of supersaturations that indicate morphological transformations in the measurements can be partially explained by individual crystals growing by dislocations or step-nucleation. Individual crystals may also grow by combinations of these mechanisms, and other mechansims such as stacking-fault generated steps, which would add to the richness and breadth of the measured range for morphological transformations. Indeed, this conclusion is consistent with the speculation of Bacon et al. (2003) that differences in growth mechanisms may have been responsible for the large range of σ_{thr} in their measurements. It is

worth noting that relatively large differences in s_{crit} for the basal and prism faces, as occurs at temperatures above -20°C, can also contribute strongly to the breadth of σ_{thr}.

Bacon et al. (2003) used their measured threshold for morphological transformation to infer s_{crit} at temperatures between -15 and -30°C, and the same can be done at temperatures below -40°C using the criterion given by Eq. 5. Wood et al. (2001) noted that faceting instability begins when the ratio between the threshold supersaturation and critical supersaturation $s_{thr}/s_{crit} \simeq 4$ for crystals grown by dislocations that transition to step nucleation. The model calculations of $\Delta\rho_{thr}$ using the s_{crit} data of Zhang and Harrington (2014) predict that $s_{thr}/s_{crit} \simeq 5$ for the fastest growing (basal) facet at a temperature of -39°C. This ratio is approximately constant from -20 to -40°C. For the slowest growing (prism) face, this ratio is $s_{thr}/s_{crit} \simeq 2.5$. It is therefore possible to use these ratios along with σ_{thr} (Eq. 5) to extend the s_{crit} estimates of Zhang and Harrington (2014) to lower temperatures. Note that for consistency with the simulations at -39°C, we use σ_{thr} = 0.326 predicted by the model (solid green line, Fig. 10). The estimates of s_{crit} at temperatures below -40°C are shown on Fig. 3 as the black squares. The error bars were computed by using the lower and upper ranges for σ_{thr} of 0.2 and 0.4, respectively. The estimated values of s_{crit} are about a factor of 2 lower than those of Harrington et al. (2019). Not surprisingly, when these s_{crit} are used in the model to predict the onset of faceting instability at temperatures below -40°C, the results follow the measurements (dotted green lines, Figs. 9 and 10). We note in passing that if the measurement-based values of σ_{thr} is used to estimate an average s_{crit} from -5 to -65°C that the resulting curve follows closely the s_{crit} data from Zhang and Harrington (2014) (not shown). This result should be expected given that the value of σ_{thr} predicted by the model at temperatures above -40°C closely follow Eq. 5.

5. Summary and Concluding Remarks

In this manuscript we revisited the excess vapor density criterion ($\Delta\rho_{thr}$) needed for the initiation of morphological transformations on the surfaces of small ice crystals. Prior measurements and observations indicate that ice crystals transform from relatively compact, solid forms to forms with complexity that increases commensurately with the supersaturation (Kobayashi 1961; Frank 1982; Bacon et al. 2003). At temperatures above about -25°C, this transformation appears to occur when the excess vapor density, $\Delta\rho_v$, exceeds approximately 0.05 g m^{-3}. At lower temperatures (below

about -40°C), morphological transformations seem to occur once the supersaturation exceeds about 20% (Bailey and Hallett 2004; Schnaiter et al. 2016). We used laboratory growth measurements (Pokrifka et al. 2023) of small ice crystals to derive a new criterion for the initiation of morphological transformations on ice crystals. This new criterion is expressed in terms of the relative excess vapor density, σ, which is the excess vapor density relative to the value at liquid equilibrium. The work of Pokrifka et al. (2023) showed that measured crystal growth rates were similar to, or lower than, those of a compact crystal (solid sphere) if $\sigma < 0.2$. Growth rates became increasingly greater than a solid sphere for $\sigma > 0.4$ indicating the existence of complex habit forms with hollowed regions and branching arms. A value of $\sigma \simeq 0.27$ approximately separated the compact from the complex growth forms. This threshold value of σ (called σ_{thr}) and its range (0.2 to 0.4) approximately delineates compact from complex crystal growth forms generated in laboratory experiments and across a wide range of temperatures (about -65 to -5°C). It also reproduces the classical threshold value of $\Delta\rho_{thr}$= 0.05 g m^{-3} at temperatures above -25°C, and it tends towards a supersaturation of about 20% at temperatures below -40°C.

The criterion for $\Delta\rho_{thr}$ put forth in this manuscript is entirely empirical, and though it is not completely necessary we attempted to find theoretical backing for this criterion. Theoretical calculations with various models (Yokoyama 1993; Nelson and Baker 1996; Wood et al. 2001) show that morphological transformations occur as the supersaturation increases. These calculations suggest that steps nucleated near crystal corners and edges drive a transformation that initially produces hollowing, followed by branching arms and side-branching (Frank 1982; Nelson 2005). We hypothesize that the excess vapor density at which hollowing begins is a reasonable proxy for when crystals should begin to transform from compact to complex forms. Theoretical calculations for the initiation of faceting instability, and therefore hollowing, compared well with the criterion for morphological transformations ($\Delta\rho_{thr}$) derived from measurements. This comparison was favorable at temperatures down to -40°C only if the critical supersaturations of Nelson and Knight (1998) and Libbrecht (2003) as compiled by Zhang and Harrington (2014) were used in the calculations. Other s_{crit} values (Harrington et al. 2019; Llombart et al. 2020) produced $\Delta\rho_{thr}$ at lower temperatures (< -20°C) that were either too high or too low. No direct measurements of s_{crit} are available at temperatures below -40°C to compare against. Given the relatively strong correspondence between the measured $\Delta\rho_{thr}$ and the model predicted value using the s_{crit} data

from Zhang and Harrington (2014), we were able to use the model predictions to estimate s_{crit} at temperatures below -40°C. The estimated values of s_{crit} are a factor of 2 lower than those estimated by Harrington et al. (2019). A number of measurements indicate that morphological transformations take place over a relatively broad range of $\Delta\rho_{thr}$ (Colbeck 1983; Bacon et al. 2003) and our measurements show this as well (Pokrifka et al. 2023). Bacon et al. (2003) argued that this relatively broad range may be due to different and diverse growth mechanisms operating on individual growing crystals, and our calculations using dislocation and step-nucleation mediated growth are consistent with this conclusion.

Though the calculations with the model of Wood et al. (2001) compare favorably with the data on hollowing and on morphological transformations in general, one should keep in mind the inherent limitations of this framework. Fundamentally, the model assumes faceted growth of single crystals only. Polycrystalline ice, such as that shown in Fig. 1, cannot be modeled with this approach. How the various facets on polycrystalline ice would affect the vapor diffusion field, and therefore the surface supersaturation is not known, though we should expect some impact. Furthermore, the model assumes a single dislocation situated at the facet center. Multiple dislocations can cause increases in the density of steps (Burton et al. 1951), and therefore the growth rate. The surface supersaturation may therefore be reduced for crystals with multiple surface dislocations, which would impact when faceting instabilities occur. Steps are not explicitly modeled, rather their effect is included through an equation for the deposition coefficient at the step sources (facet middle or corner). The deposition coefficient and surface supersaturation are determined at other locations by enforcing a constant flux boundary condition. The model cannot treat a complex surface that may include features like stacking faults that are known to occur in real crystals. It is therefore best to view the values of $\Delta\rho_{thr}$ predicted by the model as qualitative estimates of when morphological transformations may occur.

It is important to note that in-situ observations do not entirely support the laboratory-based finding that crystal complexity increases commensurately with supersaturation, with some studies showing no correlation (Ulanowski et al. 2014) and others showing a weak correlation (Järvinen et al. 2018a). This latter results is perhaps not surprising, given that crystals in real cloud systems undergo growth in a changing environment, which will alter the surface growth characteristics and complexity of the crystals. Indeed, Nelson (2008) argued theoretically that variations in

atmospheric trajectories could explain the observed range of diversity in snow. Sublimation cycles, in particular, will decrease the degree of organized surface features (Nelson 1998; Magee et al. 2014) and subsequent increases in supersaturation that produce facet regrowth (Nelson and Swanson 2019) will alter the complexity of crystals (Voigtländer et al. 2018). Unfortunately, it is not presently possible to numerically model how diverse atmospheric trajectories influence the spectrum of ice crystal growth habits in the atmosphere, so it is difficult to quantify the differences between laboratory measurements and in-situ observations.

The empirical criterion for $\Delta\rho_{thr}$ provided in this manuscript may prove useful for numerical cloud models. Some numerical cloud models require that an excess vapor density threshold be exceeded before the effective density of crystals begins to decline (Chen and Lamb 1994; Hashino and Tripoli 2007; Chen and Tsai 2016; Jensen et al. 2017). In some of these approaches, a threshold of 0.05 g m^{-3} is used and this would produce solid ice at temperatures below -30°C. The empirical form for $\Delta\rho_{thr}$ proposed herein could be used in the above cited modeling frameworks. Other approaches tend to use a size-limit based approach for transforming from compact crystals to more complex forms (Walko et al. 1995; Jensen et al. 2017), and some of these approaches are based on prior studies that suggested size was the primary determinant for when crystals begin hollowing (c.f. Mason 1993). Given that the laboratory data show a primary supersaturation dependence to the emergence of complex crystal forms, it may be well worth revisiting the definitions of smaller, pristine ice categories in numerical cloud models.

Acknowledgments. The authors are grateful for support through grants from the National Science Foundation (AGS-2128347) and the Department of Energy Atmospheric Systems Research program (DE-SC00138221). The authors appreciate insightful conversations on some of these topics with Drs. Alexei Korolev, Nathan Magee, and Israel Silber. The authors benefited from the careful critique provided by the anonymous reviewers. They are gratefully acknowledged.

Data availability statement. Older data from prior publications were extracted with the software, Engauge Digitizer and are available through Data Comments, The Pennsylvania State University at https://doi.org/10.26208/YMMC-Z637. The laboratory data used in this manuscript are available through Data Commons, The Pennsylvania State University, at https://doi.org/10.26208/htw5-q166. Ice crystal images from the ICE-Ball field campaign are available from the Department of Energy Atmospheric Radiation Measurement data archive.

References

Asakawa, H., G. Sazaki, E. Yokoyama, K. Ngashima, and S. Nakatsubo, 2014: Roles of surface/volume diffusion in the growth kinetics of elementary spiral steps on ice basal faces grown from water vapor. *Cryst. Growth Des.*, **14**, 3210–3220.

Bacon, N., M. Baker, and B. Swanson, 2003: Initial stages in the morphological evolution of vapour-grown ice crystals: A laboratory investigation. *Quart. J. Roy. Meteor. Soc.*, **129**, 1903–1927.

Bailey, M., and J. Hallett, 2004: Growth rates and habits of ice crystals between -20 and -70°c. *J. Atmos. Sci.*, **61**, 514–544.

Barrett, J. W., H. Garcke, and R. Nümberg, 2012: Numerical computations of faceted pattern formation in snow crystal growth. *Phys. Rev. E*, **86**, DOI:10.1103/PhysRevE.86.011 604.

Berg, W. F., 1938: Crystal growth from solutions. *Proceedings of the Royal Society of London, A*, **164**, 79–95.

Burton, W. K., N. Cabrera, and F. C. Frank, 1951: The growth of crystals and the equilibrium structure of their surfaces. *Philosophical Transactions of the Royal Society of London. Series A, Mathematical and Physical Sciences*, **243 (866)**, 299–358.

Chen, J., and D. Lamb, 1994: The theoretical basis for the parameterization of ice crystal habits: Growth by vapor deposition. *J. Atmos. Sci.*, **51**, 1206–1221.

Chen, J., and T.-C. Tsai, 2016: Triple-moment modal parameterization for the adaptive growth habit of pristine ice crystals. *J. Atmos. Sci.*

Colbeck, S. C., 1983: Ice crystal morphology and growth rates at low supersaturations and high temperatures. *J. Appl. Phys.*, **5 (2677-2682)**.

Frank, F. C., 1982: Snow crystals. *Contemporary Physics*, **23 (1)**, 3–22, https://doi.org/10.1080/00107518208231565.

Fukuta, N., 1969: Experimental studies on the growth of small ice crystals. *J. Atmos. Sci.*, **26**, 522–531.

Fukuta, N., and T. Takahashi, 1999: The growth of atmospheric ice crystals: A summary of findings in vertical supercooled cloud tunnel studies. *J. Atmos. Sci.*, **56**, 1963–1979.

Gonda, T., and H. Gomi, 1985: Morphological instability of polyhedral ice crystals growing in air at low temperature. *Annals of Glaciology*, **6**, 222–224.

Gonda, T., and T. Koike, 1982: Growth rates and growth forms of ice crystals grown from the vapor phase. *J. Crystal Growth*, **56**, 259–264.

Gonda, T., and T. Koike, 1983: Growth mechanisms of single ice crystals growing at low temperature and their morphological stability. *J. Crystal Growth*, **65**, 36–42.

Gonda, T., T. Sei, and H. Gomi, 1984: Growth forms and growth mechanisms of single snow crystals growing at low temperature. *Mem. Natl. Inst. Polar Res.*, **34**, 87–95.

Gonda, T., and T. Yamazaki, 1982: Morphological stability of polyhedral ice crystals growing from the vapor phase. *J. Crystal Growth*, **60**, 259–263.

Gonda, T., and T. Yamazaki, 1984: Initial growth forms of snow crystals growing from frozen cloud droplets. *J. Meteorol. Soc. Japan*, **62**, 190–192.

Hallett, J., and B. J. Mason, 1958: The influence of temperature and supersaturation on the habit of ice crystals grown from the vapor. *Proceedings of the Royal Society of London, A*, **247**, 440–453.

784 Harrington, J., and N. Magee, 2023: Ice cryo-encapsulation balloon (Project ICEBall) field cam-
785 paign report. Tech. rep., Department of Energy, ARM User Facility, DOE/SC-ARM-23-021.
786 10.2172/1974397.

787 Harrington, J., and G. Pokrifka, 2021: Approximate models for lateral growth on ice crystal
788 surfaces during vapor depositional growth. *J. Atmos. Sci.*, **78**, 967–981.

789 Harrington, J. Y., A. Moyle, L. E. Hanson, and H. Morrison, 2019: On calculating deposition
790 coefficients and aspect-ratio evolution in approximate models of ice crystal vapor growth. *Journal*
791 *of the Atmospheric Sciences*, **76 (6)**, 1609–1625, https://doi.org/10.1175/JAS-D-18-0319.1.

792 Harrison, A., A. Moyle, M. Hanson, and J. Harrington, 2016: Levitation diffusion chamber
793 measurements of the mass growth of small ice crystals from vapor. *J. Atmos. Sci.*, **73**, 2743–
794 2758.

795 Hashino, T., and G. J. Tripoli, 2007: The spectral ice habit prediction system (SHIPS). Part I: Model
796 description and simulation of the vapor deposition process. *J. Atmos. Sci.*, **64**, 2210–2237.

797 Humphreys-Owen, S., 1949: Crystal growth from solution. *Proc. R. Soc. Lond. A*, **197**, 218–237.

798 Järvinen, E., H. Wernli, and M. Schnaiter, 2018a: Investivations of mesoscopic complexity of
799 small ice crystals in midlatitude cirrus. *Geophys. Res. Let.*, **45**, 11,465–11,472.

800 Järvinen, E., and Coauthors, 2018b: Additional global climate cooling by clouds due to ice crystal
801 complexity. *Atmos. Chem. Phys.*, **18**, 15 767–15 781.

802 Jensen, A., J. Harrington, H. Morrison, and J. Milbrandt, 2017: Predicting ice shape evolution in
803 a bulk microphysics model. *J. Atmos. Sci.*, **74**, 2081–2104.

804 Kobayashi, T., 1960: Experimental researches on the snow crystal habit and growth using a
805 convection-mixing chamber. *J. Meteorol. Soc. Japan*, **38**, 231–238.

806 Kobayashi, T., 1961: The growth of snow crystals at low supersaturation. *Philosophical Magazine*,
807 **6**, 1363–1370.

808 Krämer, M., and Coauthors, 2020: A microphysics guide to cirrus – part 2: Climatologies of
809 clouds and humidity from observations. *Atmos. Chem. Phys.*, **20**, 12 569–12 608.

Kuroda, T., and R. Lacmann, 1982: Growth kinetics of ice from the vapor phase and its growth forms. *J. Cryst. Growth*, **56**, 189–205.

Lamb, K. D., J. Y. Harrington, B. W. Clouser, E. J. Moyer, L. Sarkozy, V. Ebert, O. Möhler, and H. Saathoff, 2023: Re-evaluating cloud chamber constraints on depositional ice growth in cirrus clouds – part 1: Model description and sensitivity tests. *Atmospheric Chemistry and Physics Discussions*, **23**, 6043–6064, URL https://doi.org/10.5194/acp-23-6043-2023.

Lawson, R., and Coauthors, 2019: A review of ice particle shapes in cirrus formed in situ and in anvils. *J. Geophys. Res.*, **124**, https://doi.org/ 10.1029/2018JD030 122.

Libbrecht, K., 2003: Growth rates of the principal facets of ice between -10°C and -40°C. *J. Crystal Growth*, **247**, 530–540.

Libbrecht, K. G., 2005: The physics of snow crystals. *Rep. Prog. Physics*, **68**, 855–895.

Libbrecht, K. G., 2013: An edge-enhancing crystal growth instability caused by structure-dependent attachment kinetics. *arXiv Materials Science*.

Libbrecht, K. G., 2017: Physical dynamics of ice crystal growth. *Ann. Rev. Materials Res.*, **47**, 271–295.

Llombart, P., E. Noya, and L. MacDowel, 2020: Surface phase transitions and crystal habits of ice in the atmosphere. *Science Advances*, **6**, DOI: 10.1126/sciadv.aay9322.

MacKenzie, A., and P. Haynes, 1992: The influence of surface kinetics on the growth of stratospheric ice crystals. *J. Geophys. Res.*, **97**, 8057–8064.

Magee, N., A. Miller, M. Amaral, and A. Cumiskey, 2014: Mesoscopic surface roughness of ice crystals pervasive across a wind range of ice crystal conditions. *Atmos. Chem. Phys.*, **14**, 12 357–12 371.

Magee, N., A. Moyle, and D. Lamb, 2006: Experimental determination of the deposition coefficient of small cirrus-like crystals near -50 °C. *Geophys. Res. Let.*, L17813.

Magee, N., and Coauthors, 2021: Captured cirrus ice particles in high definition. *Atmos. Chem. Phys.*, **21**, 7171–7185.

Marshall, J., and M. Langleben, 1954: a Theory of Snow-Crystal Habit and Growth. *Journal of Atmospheric Sciences*, **11**, 104–120.

Mason, B. J., 1953: The growth of ice crystals in a supercooled water cloud. *Quarterly Journal of the Royal Meteorological Society*, **79**, 104–111.

Mason, B. J., 1993: Growth habits and growth rates of snow crystals. *Proc. R. Soc. Lond. A*, **441 (3-16)**.

Miller, T., and K. Young, 1979: A numerical simulation of ice cyrstal growth from the vapor phase. *J. Atmos. Sci.*, **36**, 458–469.

Murata, K., K. Nagashima, and G. Sazaki, 2019: How do ice crystals grow inside quasiliquid layers? *Phys. Rev. Lett.*, **122**, DOI: 10.1103/PhysRevLett.122.026 102.

Nakaya, U., 1951: The formation of ice crystals. *The Compendium of Meteorology*, **1**, 207–220.

Nakaya, U., 1954: *Snow Crystals, Natural and Artificial*. Harvard University Press.

Nelson, J., 1994: A Theoretical Study of Ice Crystal Growth in the Atmosphere. Ph.D. thesis, University of Washington, 183pp.

Nelson, J., 1998: Sublimation of ice crystals. *J. Atmos. Sci.*, **55**, 910–919.

Nelson, J., 2001: Growth mechanisms to explain the primary and secondary habits of snow crystals. *Philos. Mag. A.*, **81**, 2337–2373.

Nelson, J., 2005: Branch growth and sidebranching in snow crystals. *Crystal Growth and Design*, **5**, 1509–1525.

Nelson, J., 2008: On the diversity of falling snow. *Atmos. Chem. Phys.*, **8**, 5669–5682.

Nelson, J., and M. Baker, 1996: New theoretical framework for studies of vapor growth and sublimation of small ice crystals in the atmosphere. *J. Geophys. Res.*, **101**, 7033–7047.

Nelson, J., and C. Knight, 1998: Snow crystal habit changes explained by layer nucleation. *J. Atmos. Sci.*, **55**, 1452–1465.

Nelson, J., and B. Swanson, 2019: Lateral facet growth of ice and snow – Part 1: Observations and applications to secondary habits. *Atmospheric Chemistry and Physics*, **19**, 15 285–15 320.

Neshyba, S., J. Adams, K. Reed, P. M. Rowe, and I. Gladich, 2016: A quasi-liquid mediated continuum model of faceted ice dynamics. *Journal of Geophysical Research: Atmospheres*, **121 (23)**, 14,035–14,055, https://doi.org/10.1002/2016JD025458.

Parungo, F. P., and H. K. Weickmann, 1973: Growth of ice crystals from frozen droplets. *Beitrage zur Physik der Atmosphare*, **46**, 289–304.

Pimpinelli, A., and J. Villain, 1998: *Physics of Crystal Growth*. Cambridge University Press.

Pitter, R., and H. Pruppacher, 1973: A wind tunnel investigation of freezing of small water drops falling at terminal velocity in air. *QJRMS*, **99**, 540–550.

Pokrifka, G. F., A. M. Moyle, and J. Y. Harrington, 2023: Effective density derived from laboratory measurements of the vapor growth rates of small ice crystals at -65°c to -40°c. *J. Atmos. Sci.*, **80**, 501–517.

Rottner, D., and G. Vali, 1974: Snow crystal habit at small excesses of vapor density over ice saturation. *J. Atmos. Sci.*, **31 (560-569)**.

Schmitt, C. G., and A. J. Heymsfield, 2007: On the occurrence of hollow bullet rosette- and column-shaped ice crystals in mid-latitude cirrus. *J. Atmos. Sci.*, **64**, 4524–4519.

Schnaiter, M., and Coauthors, 2016: Cloud chamber experiments on the origin of ice crystal complexity in cirrus clouds. *Atmos. Chem. Phys.*, **16**, 5091–5110.

Smith, H. R., P. Connolly, A. J. Baran, E. Hesse, A. R. D. Smedley, and A. R. Webb, 2015: Cloud chamber laboratory investigations into the scattering properties of hollow ice particles. *Journal of Quantitiative Spectropscopy and Radiative Transfer*, **157**, 106–1118.

Takahashi, C., and M. Mori, 2006: Growth of snow crystals from frozen water droplets. *Atmospheric Research*, **82**, 385–390.

Takahashi, T., T. Endoh, G. Wakahama, and N. Fukuta, 1991: Vapor diffusional growth of free-falling snow crystals between -3 and -23°c. *J. Meteorol. Soc. Japan*, **69**, 15–30.

Ulanowski, Z., P. H. Kaye, E. Hirst, R. S. Greenaway, R. J. Cotton, E. Hesse, and C. T. Collier, 2014: Incidence of rough and irregular atmospheric ice particles from Small Ice Dtector 3 measurements. *Atmos. Chem. Phys.*, **14**, 1649–1662.

889 Voigtländer, J., and Coauthors, 2018: Surface roughness during depositional growth and sublima-
890 tion of ice crystals. *Atmos. Chem. Phys.*, **18**, 13 687–13 702.

891 Walko, R. L., W. R. Cotton, M. P. Meyers, and J. Y. Harrington, 1995: New RAMS cloud
892 microphysics parameterization. Part I: The single moment scheme. *Atmos. Res.*, **38**, 29–62.

893 Wood, S., M. Baker, and D. Calhoun, 2001: New model for the vapor growth of hexagonal ice
894 crystals in the atmosphere. *J. Geophys. Res.*, **106**, 4845–4870.

895 Wood, S. E., M. B. Baker, and B. D. Swanson, 2002: Instrument for studies of homogeneous
896 and heterogeneous ice nucleation in free-falling supercooled water droplets. *Review of Scientific*
897 *Instruments*, **73**, 3988–3996.

898 Yamashita, A., 1976: Growth processes of ice crystals and a low which related to the symmet-
899 ric growth of plate-like snow crystals. *Proceedings of the International Conference on Cloud*
900 *Physics*, Boulder, CO, American Meteorological Society.

901 Yokoyama, E., 1993: Formation of patterns during growth of snow crystals. *J. Crystal Growth*,
902 **128**, 251–257.

903 Zhang, C., and J. Harrington, 2014: Including surface kinetic effects in simple models of ice vapor
904 diffusion. *J. Atmos. Sci.*, **71**, 372–390.